Research article

Mutasem Odeh, Matthieu Dupré, Kevin Kim and Boubacar Kanté*

Optical response of jammed rectangular nanostructures

https://doi.org/10.1515/nanoph-2020-0431
Received July 28, 2020; accepted October 12, 2020;
published online November 24, 2020

Abstract: Random jammed dipole scatterers are natural composite and common byproducts of various chemical synthesis techniques. They often form complex aggregates with nontrivial correlations that influence the effective dielectric description of the medium. In this work, we investigate the packing dynamic of rectangular nanostructure under a close packing protocol and study its influence on the optical response of the medium. We show that the maximum packing densities, maximum scattering densities, and percolation threshold densities are all interconnected concepts that can be understood through the lens of Onsager's exclusion area principle. The emerging positional and orientational correlations between the rectangular dipoles are studied, and various geometrical connections are drawn. The effective dielectric constants of the generated ensembles are then computed through the strong contrast expansion method, leading to several unintuitive results such as scattering suppression at maximum packing densities, as well as densities below the percolation threshold, and maximum scattering in between.

Keywords: disorder; metamaterials; metasurfaces; nanostructures.

***Corresponding author: Boubacar Kanté**, Department of Electrical Engineering and Computer Sciences, University of California, Berkeley, CA 94720, USA; and Department of Electrical and Computer Engineering, University of California San Diego, La Jolla, CA 92093, USA; and Materials Sciences Division, Lawrence Berkeley National Laboratory, 1 Cyclotron Road, Berkeley, California 94720, USA, E-mail: bkante@berkeley.edu. https://orcid.org/0000-0001-5633-4163
Mutasem Odeh, Department of Electrical Engineering and Computer Sciences, University of California, Berkeley, CA 94720, USA
Matthieu Dupré and Kevin Kim, Department of Electrical and Computer Engineering, University of California San Diego, La Jolla, CA 92093, USA

1 Introduction

Random packing persists to be an alluring topic, pertinent to fundamental questions in physics, chemistry, and biology [1–3]. Within the field of optics and photonics, in particular, understanding light–matter interactions in random packed media is crucial and urged by the growing usage of optical sensors and imaging systems in probing complex living cells, liquids, and granular media. In addition, the thriving genre of disordered photonics domesticates randomness toward various applications in light trapping [4], radiative cooling [5], and random lasing [6].

In this work, we investigate the optical response of packed rectangular nanostructures on a surface, as they are commonly employed as dipole scatterers in optical devices [7–9] for various applications including light harvesting [10] and biosensing [11]. However, a detailed electromagnetic simulation of such an ensemble is a computationally expensive task to perform and one rather seeks the effective medium description as an approximation. Many homogenization theories with varying degrees of applicability and complexity have been developed toward this aim [12, 13]. Bruggeman's theory models aggregate structure with constituents that are treated on an equal footing and therefore cannot be applied in this case [14]. Maxwell–Garnett approximation, on the other hand, models inclusions dispersed in a continuous host medium. Its analytic simplicity arises from the consideration of only the one-point probability function (density) where convergence is assured under the dilute and long wavelength limit. However, at large packing density, the positional and orientational correlations between the dipoles are not negligible anymore and can drastically alter the effective dielectric constant of the ensemble. The *strong contrast expansion method* presented in the study by Rechtsmanand and Torquato [13] is rather a generic and exact approach that includes the contribution of high-order point probability functions and thus captures the correction due to the emerged correlations.

In this article, we investigate the influence of the packing dynamic on the optical response of jammed rectangular

nanostructures. A comprehensive workflow chart can be found in the supplementary material (section S1). In section 2, we define the packing protocol used in the study and compute the maximum achieved packing densities at various aspect ratios. We proceed in section 3 with point process statistical analysis to unravel the short-range ordering and spontaneous alignment between the packed rectangles. In section 4, we model the ensemble as a two-phase isotropic medium and estimate the effective dielectric constant (ε_{eff}) using the strong contrast expansion method. The last section concludes and summarizes the work.

2 Random close packing

We consider the packing of hard rectangles of length l and width w on a square substrate, where the interaction potential $\phi(x)$ is infinite inside the rectangle region and zero otherwise. Therefore, a stable state is a state with no overlapping elements. The maximum packing density and the state characteristics are protocol dependent. In this work, we implement a collective rearrangement packing protocol which models an abrupt surge or sedimentation of the rectangle concentration near an adsorbing edge which is common in many chemical synthesis techniques [15, 16]. The algorithm starts by placing N identical rectangles of aspect ratio $\alpha = l/w$ at random positions and orientations on a flat substrate of area A_s with an initial packing fraction $\phi_i = Nlw/A_s$, as shown in Figure 1A. In an iterative procedure, each overlapping rectangle is individually displaced from its initial position with a random radial distance and orientation that are uniformly distributed on the range of $[0, 2l]$ and $[0, \pi]$, respectively. The procedure persists until the rectangle avoids overlapping or n attempts has been reached after which the process is terminated, and the rectangle is removed from the packing process. To calculate the maximum packing density ($\phi_{\max}$), we configured the initial density to $\phi_i = 0.6$, number of attempts to $n = 100{,}000$, and particle number to $N = 10{,}000$. Periodic boundaries were used to avoid finite size effects, and the results were averaged over multiple realizations to ensure convergence. The maximum packing density achieved for different aspect ratios is shown in Figure 1B. We note that $\phi_{\max}$ is aspect ratio dependent with a unique cusp around $\alpha = 1.5$. The decrease of $\phi_{\max}$ to the right of the cusp can be explained through the lens of Onsager's exclusion area principle [17]. The principle states that each rectangle has an excluding area $A(l, w, \theta)$ within which other similar rectangles with a relative angel θ are forbidden to occupy if overlapping is to be avoided, as illustrated by the inset in Figure 1B. The ratio of the

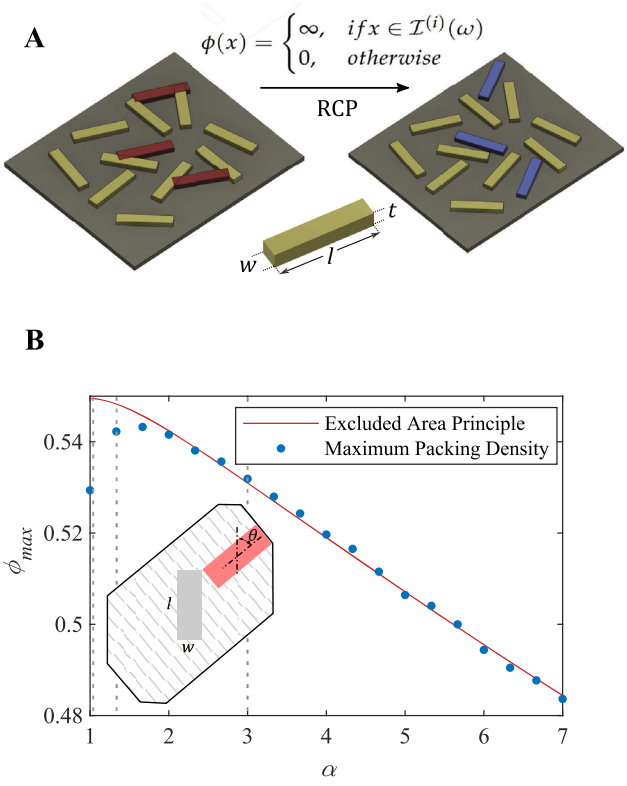

Figure 1: Random close packing of hard rectangles: (A) illustration of the collective rearrangement packing protocol with $\phi(x)$ as the interaction potential and $I^{(i)}(\omega)$ is the indicator function of phase i in realization ω and (B) is the computed maximum packing density ($\phi_{\max}$) as a function of the aspect ratios (α). The blue dots represent the simulated data, and the red curve is a fitting line based on the excluded area principle given by Eq. (1) with $c_1 = 0.047$ and $c_2 = 1.725$. The inset illustrates the excluded area of a rectangle of length l and width w with another identical rectangle with a relative tilt θ.

rectangle area lw to what it excludes on average $\langle A \rangle$ across all probable angels $[0, \pi]$ has been shown to give an accurate estimation of the percolation threshold [18] and is given by the following equation:

$$\phi_{\max}(\alpha) = \frac{lw}{\langle A \rangle} = \frac{\alpha}{c_1(1+\alpha^2) + c_2\alpha} \tag{1}$$

where $c_1 = 2/\pi$ and $c_2 = (2 + 8/\pi)$ in the case of penetrable rectangles. However, our protocol induces a nontrivial positional and orientational correlation that makes the excluded area principle difficult to be derived for $\phi_{\max}$ estimation. In fact, this is the parking problem in 2D which is still an open question to be answered. Nonetheless, we found that the behavior can still be well captured by Eq. (1), using a fitted value of the c_1 and c_2 coefficients, as shown in Figure 1B. However, the model fails to fit the cusp and $\phi_{\max}$ at low aspect ratios. Similar behavior has been observed for

packing hard ellipsoids, explained through the isostatic conjecture, and verified through the famous *M&M's* experiment [19, 20]. The conjecture states that the mean contact number between packed elements is on average twice the number of degrees of freedom in a jammed configuration. Consequently, deviating from squares to rectangles introduces an additional degree of freedom (orientation) to the packing process, which increases the average contact numbers and consequently $\phi_{\max}$. Strictly speaking, our packing protocol does not lead to a jammed state rather than a saturated state with an average contact number of zero. Nonetheless, the state can still be treated as a jammed one since the element cannot move once they settled on a nonoverlapping position [20]. Therefore, there are two competing effects occurring in the close packing protocol. On the one hand, adding an extra degree of freedom to squares gives extra flexibility to pack at higher densities (isostatic conjecture), yet on the other hand, increasing the degree of anisotropy prevents short-range ordering and limits the maximum packing density instead (exclusion area principle). These behaviors have a direct influence on the effective dielectric constant of the random jammed media. For example, engineering a random medium with high dielectric constant requires, in general, a high density of packed rectangles. Unintuitively, this can be optimally approached by choosing rectangles of 1.5 aspect ratio, as can be deduced from Figure 1B.

3 Point process statistical analysis

The collective rearrangement packing protocol produces a statistically homogeneous medium that we assume ergodic (any single realization of the ensemble is representative of the ensemble in the infinite area-limit). We start our investigation by performing a stochastic point process analysis. Each rectangle is represented by its two midpoint coordinates (x, y) and the angle (θ) that the longer axis makes with respect to a fixed global reference. We calculate two important statistical descriptors. The first is the radial *pair correlation* function, which is defined as follows:

$$g_2(r) = \frac{\rho_2(r)}{\rho^2}, \tag{2}$$

where ρ is the number density (number of points per unit area in the infinite area limit) and $\rho_2(r)$ is the number of points within a distance of r and $r + dr$ from a reference rectangle. Thus, a deviation of $g_2(r)$ from the unity provides a measure of positional correlation or anticorrelation between the rectangles. The second statistical descriptor is the orientational correlation function $g_\theta(r)$ defined in the study by Ma and Torquato [21] as follows:

$$g_\theta(r) = <\cos(2[\theta(0) - \theta(r)])>, \tag{3}$$

which is an average measure of the degree of alignment between two rectangles within a distance of r and $r + dr$. Thus, $g_\theta > 0$ suggests statistically parallel rectangles, $g_\theta < 0$ suggests statistically perpendicular rectangles, and $g_\theta = 0$ suggests the lack of any preferential orientation. The two statistical descriptors were applied to the states of maximum packed density that were presented in Figure 1B. The width is normalized ($w = 1$) without loss of generality, and the descriptors are plotted as shown in Figure 2A and B. We observe the emergence of three distinct features on both surfaces that can be fitted by three lines (p_1, p_2, p_3) that intersect at $(\alpha = 1, r = 1)$. Transitioning from squares to rectangles causes an interesting trifurcation of the first appearing peak at $\alpha = 1$, as clarified by the top view insets of Figure 2A and B. The trifurcation is a clear sign of the isostatic conjecture. The conjecture states that in a jammed configuration, the mean contact number between packed elements is on average twice the number of degrees of freedom (DOFs) [19, 20]. For simplicity, we can approximate squares as circles and rectangles as ellipsoids by ignoring the sharp edges that have a negligible influence on the packing dynamic. Building on this approximation, there are two DOFs for squares (x, y) and three DOFs for rectangles (x, y, θ). According to the isostatic conjecture, we can conclude that the average contact number increases from 4 to 6 when deforming squares to rectangles. Consequently, the ensemble contains two extra possible configurations, that is, in addition to the original configuration, and forms the trifurcation observed in Figure 2A and B. The low g_2 correlation in the triangular region between p_1 and p_2 is a direct consequence of the excluding area principle. In other words, as the aspect ratio increases, it becomes statistically difficult to pack rectangles within close proximity. Figure 2C shows a cross-sectional plot of both g_2 and g_θ for two different aspect ratios. For the square case $(\alpha = 1)$, we note a sharp increase in g_2 at $r > 1$ indicating a high probability of occupancy. On contrary to the case of circles packing where the increase is abrupt, rectangle packing has a finite slope that is attributed to their radial asymmetry. In addition, the high probability of occupancy of the first neighbor square induces a negative correlation on the next adjacent regions, a repeated process that explains the oscillatory behavior of $g_2(r)$ that is damped with distance. We also note that g_θ is approximately zero, suggesting the lack of any preferential alignment between the packed squares. On the other hand, for $\alpha = 3$, g_θ is positively correlated in the region between p_2 and p_3, whereas g_r is negatively correlated. The statistical

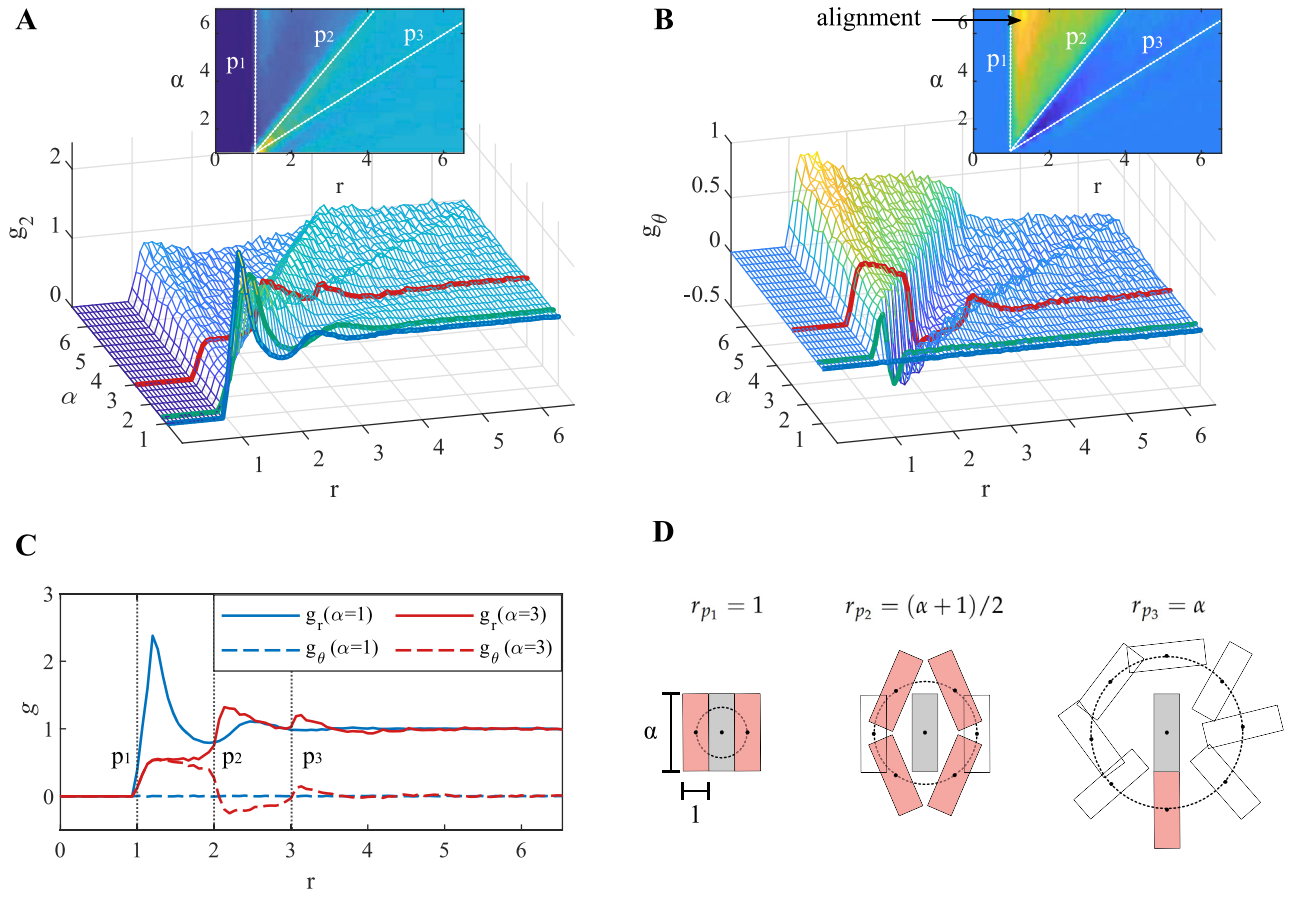

Figure 2: Point process analysis of maximally random packed rectangles:
(A) radial pair correlation functions $g_2(r,\alpha)$ given by Eq. (2) and (B) orientational correlation function $g_\theta(r,\alpha)$ given by Eq. (3). Three different aspect ratios are highlighted on both surfaces with different colors; the blue line corresponds to $\alpha = 1$, green to $\alpha = 1.3$, and red to $\alpha = 3$. The insets on both surfaces correspond to a top view perspective with three important features highlighted by p_1, p_2, p_3 lines. (C) A cross sectional plot of g_2 and g_θ surfaces at $\alpha = 1$ and $\alpha = 3$ and (D) geometrical illustration of the origin of p_1, p_2, p_3 lines, respectively. For each configuration, the dashed circle with radius r_{pi} represents the shortest distance between rectangles' center for overlap to be avoided.

interpretation indicates that it is highly constrained to place two rectangles in proximity, yet if it is deemed necessary, they must be well aligned. However, such constraint is lifted at p_2 and further relaxed at p_3. The three constraints can be traced geometrically, as illustrated in Figure 2D. The p_2 line equals to the minimum distance when two perpendicular rectangles are not overlapping, that is, when $r_{p_2} = (\alpha+1)/2$. The p_3 line equals to the minimum distance of two stacked rectangles on their longer axes, that is, when $r_{p_3} = \alpha$. We also note that at each relaxation point (p_1, p_2, p_3), a transition in the sign of g_θ occurs.

We conclude from this analysis the lack of long-range translational or nematic order in the ensemble. The effective permittivity in the 2D plane is thus macroscopically isotropic and polarization independent at all aspect ratios. In addition, high aspect ratios have a destructive behavior on short-range positional order, and therefore, their scattering features will be weaker. Furthermore, the average rectangle orientation after lifting the p_2 constrain is approximately $\theta \approx \pi/4$. In the simple dipole picture, this suggests a spectral redshift for the resonance mode supported along the longer axis (h), as illustrated in the middle configuration of Figure 2D.

4 Strong contrast expansion of the effective dielectric constant

The statistical properties of phase i in two-phase heterogeneous media can be specified by an infinite set of n-point probability functions S_n^i [22]. In a homogeneous and isotropic medium, the first term reduces simply to the density of phase i ($S_1^{(i)} = \phi_i$), whereas the second term $S_2^{(i)}(r)$ is interpreted as the probability of finding both endpoints of a line segment of length r in phase i. In the

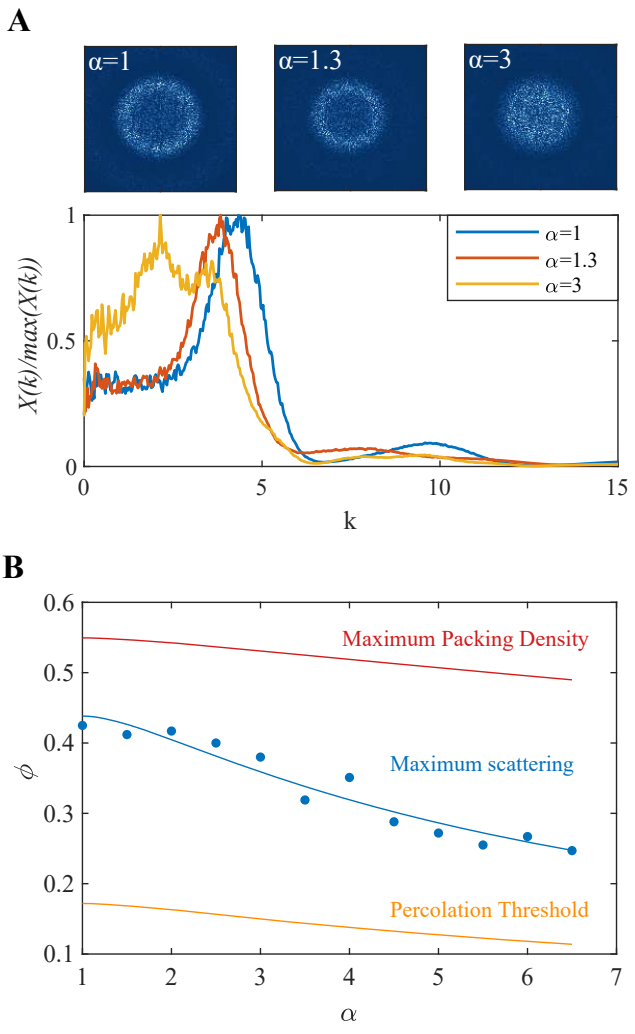

Figure 3: Two-phase heterogeneous analysis: (A) spectral density images for $\alpha = 1, 1.3, 3$ at ϕ_{max} followed by a radial average plot and (B) density plot as a function of the aspect ratio, showing three curves fitted using the excluded are principle given by Eq. (1): (i) percolation threshold curve (yellow) fitted with $c_1 = 2/\pi$ and $c_2 = (2 + 8/\pi)$ where ensembles below exhibit weak correlation; (ii) maximum scattering density curve (blue) fitted with $c_1 = 0.3780$ and $c_2 = 1.5255$ represents the ensembles at which the zeroth wavevector spectral density function $\chi_v(k = 0)$ exhibits a maximum; and (iii) the maximum packing density curve (red) fitted with $c_1 = 0.047$ and $c_2 = 1.725$.

following discussion, we will drop the superscript (i) and implicitly refer to the rectangle phase. The scattering behavior of the ensemble is captured by the spectral density function $\chi_v(k)$ which is the Fourier transform of the autocovariance function $\chi_v(r) = S_2(r) - S_1^2$. Figure 3A shows the spectral density for three different aspect ratios $(\alpha = 1, 1.3, 3)$ at their maximum packing density limit. Structures with low aspect ratios exhibit a clear attenuation in their scattering behavior at small k wave vectors. This is attributed to the suppression of long-range density fluctuations due to the positional ordering of the packed elements. The attenuation becomes weaker as α increases due to the destructive role of the addition of an extra DOF to the packing process, as discussed previously. The scattering behavior is reminiscent of hyperuniformity where $\chi_v(k) \to 0$ as $k \to 0$ [23]. Hyperuniform structures have been shown to exhibit unique optical properties including the formation of isotropic photonic bandgap that can be used for light guiding and confinement [24, 25]. In addition, the suppressed scattering can lead to transparency in a dielectric medium [26] and enhanced optical absorption in a lossy medium [27]. Although, strictly speaking, our packing dynamic does not lead to hyperuniform structure $(\chi_v(k) \neq 0$ as $k \to 0)$, shared properties are expected. Given that the scattering is weak below the percolation threshold due to the low number of scatterers and similarly weak at maximum packing densities due to the suppression of long-range fluctuations, we expect that there should be an intermediate regime where the scattering events are maximum. We evaluated the zeroth wavevector spectrum density function $\chi_v(k = 0)$ for different aspect ratios (α) and located the densities at which the function is maximum, as shown in Figure 3B. Indeed, such an intermediate regime exists between the percolation and maximum packing density limits. In addition, its aspect ratio dependence can also be fitted by the exclusion area principle using Eq. (1).

From the calculated autocovariance function, we can proceed in calculating the effective-dielectric constant by the strong contrast expansion method. The expressions presented in the study by Rechtsman and Torquato [13] were formulated for 3D random structures. We rederive the method for two-phase medium in 2D and truncate the expansions up to the second order to include the 2-point probability function $S_2^{(i)}(r)$. In addition, we focus on the effective dielectric constant experienced by a transverse magnetic plane wave propagating parallel to the 2D medium plane $(k_z = 0, E_z = 0)$. The effective permittivity can be obtained from the following expression (see section S2 for full discussion):

$$\beta_{pq}^2 \phi_p^2 \beta_{eq}^{-1} = \phi_p \beta_{pq} - \underbrace{A_2^{(p)} \beta_{pq}^2}_{\text{2nd order}}, \tag{4}$$

where ϕ_p is the area density of the packed rectangles, $\beta_{pq} = (\varepsilon_p - \varepsilon_q)/(\varepsilon_p + \varepsilon_q)$ is the rectangles polarizability (phase p) with respect to the environment (phase q), and $\beta_{eq} = (\varepsilon_{\text{eff}} - \varepsilon_q)/(\varepsilon_{\text{eff}} + \varepsilon_q)$ is the effective polarizability with respect to the environment. A_2^p is the coefficient of the second-order correction for a 2D isotropic medium

$$A_2^{(p)} = \frac{i\pi k_q^2}{2} \int_0^{r_{\max}} dr\, r H_0^{(1)}(k_q r)\, \chi_V(r), \tag{5}$$

where $H_0^{(1)}$ is the Hankel function of the first kind which acts as propagator function for $\chi_V(r)$. It is important to emphasize that Eq. (5) is approximately valid when $\lambda_q \gg r_{\max}$, where λ_q is the wavelength in the background medium and $r_{\max}$ is the radius at which the positional correlation is negligible ($\chi_V(r > r_{\max}) \approx 0$). In other words, all positionally correlated dipoles are assumed to be excited in phase by an external plane wave of wavelength λ_q. However, the condition is not stringent, and an extension of the applicable wavelength range has been recently shown possible [28]. It can be noted that when $A_2^p \beta_{pq}^2$ approaches zero, the expression reduces simply to the well-known Maxwell–Garnett approximation. This is approximately valid for large wavelength ($k_q \to 0$) and short-range autocovariance function $\chi_V(r)$. In this limit, pure dielectric constituents ($\varepsilon_p, \varepsilon_q$) result in a pure effective permittivity ($\mathrm{Im}[\varepsilon_{\mathrm{eff}}] = 0$). The conditions are approximately met for subwavelength rectangles below the percolation threshold, as illustrated in Figure 3B. This is because, above the percolation threshold, the formation of an infinite sized cluster of overlapping rectangles requires many adjustments of the rectangles' positions and orientations to reach a nonoverlapping state, resulting in a long-range autocovariance function $\chi_V(r)$. The real and imaginary parts of $\varepsilon_{\mathrm{eff}}$ were evaluated as a function of wavelength for three different aspect ratios ($\alpha = 1, 1.3, 3$) at their maximum packing densities ($\phi_{\max}$), as shown in Figure 4. In the studied configurations, $\chi_V(r)$ becomes in the order of 10^{-6} for $r > 5$. Therefore, $\varepsilon_{\mathrm{eff}}$ calculated by Eq. (4) is approximately accurate for $\lambda_q \gg 5$. It can also be noted that the complex permittivity approaches the one calculated by the Maxwell–Garnett approximation as $\lambda_q \to \infty$. Furthermore, large aspect ratios damp the resonance and spread the scattering for larger wavelengths. This is consistent with power spectrum density shown in Figure 3A since there exists a proportionality between $\mathrm{Im}[\varepsilon_{\mathrm{eff}}]$ and $\chi_V(k)$ as $k \to 0$ [13].

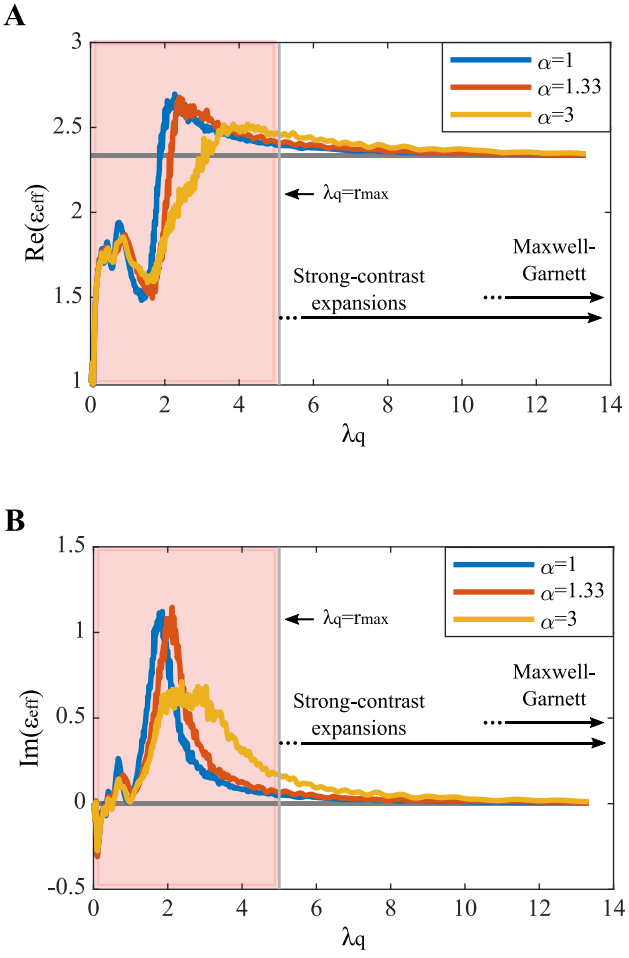

Figure 4: The complex effective dielectric constant ($\varepsilon_{\mathrm{eff}}$) for jammed rectangular nanostructures calculated by the strong contrast expansion method and plotted as a function of wavelength (λ_q). The 2D rectangles have width $w = 1$, height $h = \alpha$, permittivity $\varepsilon_p = 9$, and are maximally packed ($\phi_{\max}$) in a background medium with permittivity $\epsilon_q = 1$. (A) The real part of $\varepsilon_{\mathrm{eff}}$ showing an explicit redshift as α increases, and (B) the imaginary part of $\varepsilon_{\mathrm{eff}}$ showing larger scattering as α increases for $\lambda_q \gg r_{\max}$. In the long wavelength limit, both the real and imaginary parts of $\varepsilon_{\mathrm{eff}}$ approach the Maxwell–Garnett approximation.

5 Conclusion

Random packed media are a ubiquitous and natural outcome of various chemical synthesis techniques. In the subwavelength limit, the complex inhomogeneous medium can be described by an effective homogeneous one with great accuracy. In this work, we statistically analyze jammed rectangular dipoles under the random close packing protocol for various densities and aspect ratios. The arising microscopic correlations were traced and shown to have direct and indirect consequences on the effective dielectric constant of the medium. Statistical tools and concepts such as Onsager's excluded area principle, the positional correlation function, and the orientational correlation function, are of great utilities in describing the state of the ensemble and deduce some of the optical characteristics such as polarization dependence and spectral shifts. To study the influence of structural correlations on the macroscopic optical response, we accommodate the strong contrast expansion method to two-dimensional structure and use it to estimate the effective

dielectric constant for the generated ensembles. This allows us to capture various effects beyond what Maxwell–Garnett approximation can, such as scattering enhancement and suppression as well as correlation-induced spectral shift. This work paves a systematic path toward engineering random medium with tailored optical properties.

Author contribution: All the authors have accepted responsibility for the entire content of this submitted manuscript and approved submission.
Research funding: This work was supported by the National Science Foundation Career Award (ECCS-1554021), the Office of Naval Research Young Investigator Award (N00014-17-1-2671), the ONR JTO MRI Award (N00014-17-1-2442), and the DARPA DSO-NLM Program no. HR00111820038.
Conflict of interest statement: The authors declare no conflicts of interest regarding this article.

References

[1] J. D. Bernal, "A geometrical approach to the structure of liquids," *Nature*, vol. 183, pp. 141–147, 1959.
[2] P. Schaaf and J. Talbot, "Kinetics of random sequential adsorption," *Phys. Rev. Lett.*, vol. 62, pp. 175–178, 1989.
[3] J. Feder, "Random sequential adsorption," *J. Theor. Biol.*, vol. 87, pp. 237–254, 1980.
[4] H. Atwater and A. Polman, "Plasmonics for improved photovoltaic devices," *Nat. Mater.*, vol. 9, pp. 205–213, 2010.
[5] Y. Zhail, Y. Ma, S. David, et al., "Scalable-manufactured randomized glasspolymer hybrid metamaterial for daytime radiative cooling," *Science*, vol. 355, pp. 1062–1066, 2017.
[6] N. Lawandy, R. Balachandran, A. Gomes, et al., "Laser action in strongly scattering media," *Nature*, vol. 368, pp. 436–438, 1994.
[7] M. Dupre, L. Hsu, and B. Kante, "On the design of random metasurface based devices," *Sci. Rep.*, vol. 8, p. 7162, 2018.
[8] H. Nasari, M. Dupré, and B. Kanté, "Efficient design of random metasurfaces," *Opt. Lett.*, vol. 43, pp. 5829–5832, 2018.
[9] J. Park, A. Ndao, W. Cai, et al., "Symmetry-breaking-induced plasmonic exceptional points and nanoscale sensing," *Nat. Phys.*, vol. 16, pp. 462–468, 2020.
[10] Y.-Z. Zheng, X. Tao, J.-W. Zhang, et al., "Plasmonic enhancement of light-harvesting efficiency in tandem dye-sensitized solar cells using multiplexed gold core/silica shell nanorods," *J. Power Sources*, vol. 376, pp. 26–32, 2018.
[11] A. Abbas, L. Tian, J. J. Morrissey, et al., "Hot spot-localized artificial antibodies for label-free plasmonic biosensing," *Adv. Funct. Mater.*, vol. 23, pp. 1789–1797, 2013.
[12] M. Safdari, M. Baniassadi, H. Garmestani, et al., "A modified strong-contrast expansion for estimating the effective thermal conductivity of multiphase heterogeneous materials," *J. Appl. Phys.*, vol. 112, p. 114318, 2012.
[13] M. Rechtsman and S. Torquato, "Effective dielectric tensor for electromagnetic wave propagation in random media," *J. Appl. Phys.*, vol. 103, pp. 1–15, 2008.
[14] G. A. Niklasson, C. G. Granqvist, and O. Hunderi, "Effective medium models for the optical properties of inhomogeneous materials," *Appl. Opt.*, vol. 20, pp. 26–30, 1981.
[15] A. Bertei, C. C. Chueh, J. G. Pharoah, et al., "Modified collective rearrangement sphere-assembly algorithm for random packings of nonspherical particles: towards engineering applications," *Powder Technol.*, vol. 253, pp. 311–324, 2014.
[16] J. Perez-Justea, I. Pastoriza-Santosa, L. Liz-Marzana, et al., "Gold nanorods: synthesis, characterization and applications," *Coord. Chem. Rev.*, vol. 249, pp. 1870–1901, 2005.
[17] L. Onsager, "The effects of shape on the interaction of colloidal particles," *Ann. N. Y. Acad. Sci.*, vol. 51, pp. 627–659, 1949.
[18] I. Balberg, C. H. Anderson, S. Alexander, et al., "Excluded volume and its relation to the onset of percolation," *Phys. Rev. B*, vol. 30, pp. 3933–3943, 1984.
[19] A. Donev, I. Cisse, D. Sachs, et al., "Improving the density of jammed disordered packings using ellipsoids," *Science*, vol. 303, pp. 990–993, 2004.
[20] P. Chaikin, A. Donev, W. Man, et al., "Some observations on the random packing of hard ellipsoids," *Ind. Eng. Chem. Res.*, vol. 45, pp. 6960–6965, 2006.
[21] Z. Ma and S. Torquato, "Hyperuniformity of generalized random organization models," *Phys. Rev. E*, vol. 99, p. 022115, 2019.
[22] S. Torquato, *Random Heterogeneous Materials*, Berlin, Springer, 2002.
[23] S. Torquato, "Hyperuniform states of matter," *Phys. Rep.*, vol. 745, pp. 1–95, 2018.
[24] W. Man, M. Florescu, K. Matsuyama, et al., "Photonic band gap in isotropic hyperuniform disordered solids with low dielectric contrast," *Opt. Express*, vol. 21, pp. 19972–19981, 2013.
[25] W. Man, M. Florescu, E. P. Williamson, et al., "Isotropic band gaps and freeform waveguides observed in hyperuniform disordered photonic solids," *Proc. Natl. Acad. Sci. U.S.A.*, vol. 40, pp. 15886–15891, 2013.
[26] O. Leseur, R. Pierrat, and R. Carminati, "High-density hyperuniform materials can be transparent," *Optica*, vol. 3, pp. 763–767, 2016.
[27] F. Bigourdan, R. Pierrat, and R. Carminati, "Enhanced absorption of waves in stealth hyperuniform disordered media," *Opt. Express*, vol. 27, pp. 8666–8682, 2019.
[28] S. Torquato and J. Kim, "Nonlocal effective electromagnetic wave characteristics of composite media: beyond the quasistatic regime," arXiv preprint arXiv:2007.00701.

Supplementary Material: The online version of this article offers supplementary material (https://doi.org/10.1515/nanoph-2020-0431).